Ultrathin Dual-Band Circularly Polarized Antenna

Mingzhe Hu, Yue Li, *Senior Member, IEEE*, Yongjian Zhang, *Member, IEEE*, Pengfei Wu, and Hanyang Wang, *Fellow, IEEE*

***Abstract*—This letter presents a dual-band circularly polarized microstrip antenna with an ultrathin substrate made of liquid crystal polymer (LCP). The proposed antenna consists of a gridded patch and a round of via fence for dual-band radiation and size miniaturization. Compared with the previous designs, the proposed antenna has two improvements in structures with merits: first, a parasitic patch is added below the gridded patch to tune the ratio of dual-band frequencies; second, a stacked feeding network with dual orthogonal L-shaped probes is designed for profile reduction, also providing the feasibility of differential feed and dual-linear polarization. Based on the codesign of the gridded patch, the parasitic patch, and the stacked feeding network, all layers of the antenna are clamped into a flexible board with an ultrathin thickness of 0.6 mm ($0.013\lambda_0$, λ_0 is the free-space wavelength at 6.5 GHz) and taped out with the flexible LCP process. The measured results show the bandwidths of total efficiency over 25% are 6.25–6.74 GHz and 7.92–8.17 GHz with circular polarization, proving to be a feasible solution for flexible antennas in space-limited mobile handsets.**

***Index Terms*—Antenna feeds, circular polarization, flexible printed circuit (FPC), microstrip antennas, multiple-band antennas.**

I. Introduction

With the development of mobile communications, various applications have emerged for better user experience. Among them, the ultrawideband (UWB) technology for indoor positioning is an attractive one due to its strong penetration capabilities, insensitivity to multipath, and centimeter-level high resolution [1], [2], [3]. Many types of antennas have been proposed for UWB applications [4], [5], [6]. Specifically, dual-band circularly polarized (DBCP) antennas are widely used for stable performance. Dual-band operation helps suppress interference with other bands, and circularly polarized (CP) antennas can prevent polarization mismatch with a random direction of the device. Using dual modes of one whole or two separate radiators are common methods to realize dual-band antennas [7], [8], [9], [10]. In [7], by cutting an *S*-shaped slot on a single patch, multiple current paths are created to operate at two bands with a small frequency ratio. Two stacked patches are used in [9] and [10] to excite the dual-band radiation. Besides, by loading grid slots on a rectangular patch in [11] and [12], the antiphase TM_{20} mode is effectively excited to contribute to the wideband radiation. In [13], the stacked structure can achieve dual-band operation in millimeter-wave bands. For circular polarization, two orthogonal linearly polarized (LP) waves with an equal amplitude and a 90° phase difference can be used to form a CP wave [14], [15], [16].

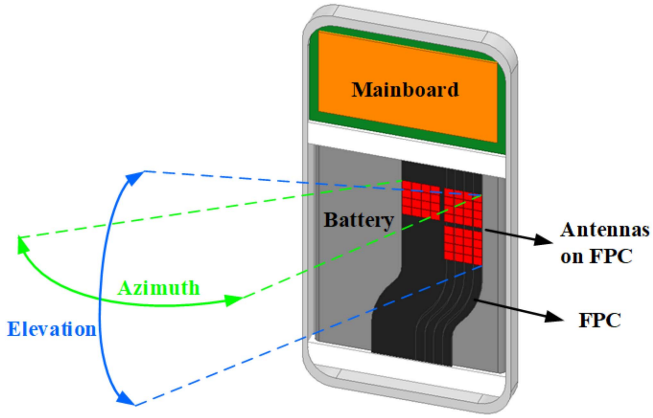

Fig. 1. Application scenario of UWB indoor positioning of the proposed antenna on FPC of mobile devices.

For antenna design in mobile handsets, size reduction is key to fitting the extreme environment. The blind via fence is loaded near the aperture of microstrip antennas as parallel capacitance, which can concentrate the E-field and, thus, realize antenna miniaturization [17], [18]. For space-limited mobile devices, the flexible printed circuit (FPC) between the battery and the back cover has been verified as an alternative to place the antenna [19]. The liquid crystal polymer (LCP) is chosen as the dielectric of the FPC [19], [20], [21]. The specific application scenario of antennas on FPC and the principle of positioning is illustrated in Fig. 1. By placing three elements on FPC in an L-shaped pattern, angle detecting in both elevational and azimuthal planes can be realized. The two horizontal elements (on the top) work for azimuthal positioning, and the two vertical elements (on the right) for elevated positioning. Due to the requirements of FPC, the antenna needs to have ultrathin profile, compact size, and integration with a complete ground.

In this letter, a DBCP microstrip antenna with an ultrathin profile of 0.6 mm ($0.013\lambda_0$, λ_0 is the free-space wavelength at 6.5 GHz) is presented. By exciting the TM_{10} mode and the antiphase TM_{20} mode of the gridded patch, a dual-band operation with broadside radiation is obtained. The parasitic patch and the via fence can help with frequency tuning and

Manuscript received 2 November 2023; accepted 1 December 2023. Date of publication 5 December 2023; date of current version 5 March 2024. This work was supported in part by the National Natural Science Foundation of China under Grant U22B2016 and Grant 62022045, and in part by Huawei Technologies. *(Corresponding author: Yue Li.)*

Mingzhe Hu, Yue Li, and Yongjian Zhang are with the Department of Electronic Engineering, Beijing National Research Center for Information Science and Technology, Tsinghua University, Beijing 100084, China (e-mail: humz22@mails.tsinghua.edu.cn; lyee@tsinghua.edu.cn; zhangyj18@tsinghua.org.cn).

Pengfei Wu is with the Department of Wireless Technology, Huawei Technology Company Ltd., Shanghai 201206, China (e-mail: wupengfei3@huawei.com).

Hanyang Wang is with Huawei Technologies (U.K.), Ltd., OX14 2HJ Abingdon, U.K. (e-mail: hanyang.wang@huawei.com).

Digital Object Identifier 10.1109/LAWP.2023.3339203

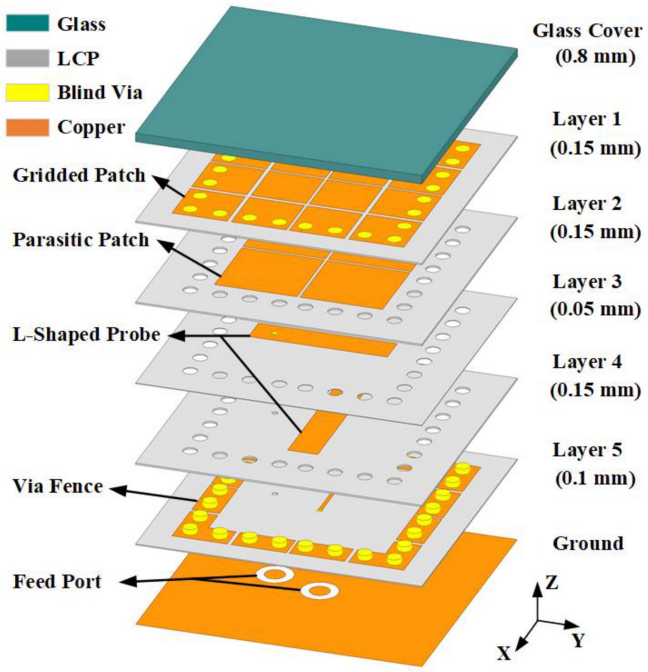

Fig. 2. Exploded view of the proposed DBCP antenna.

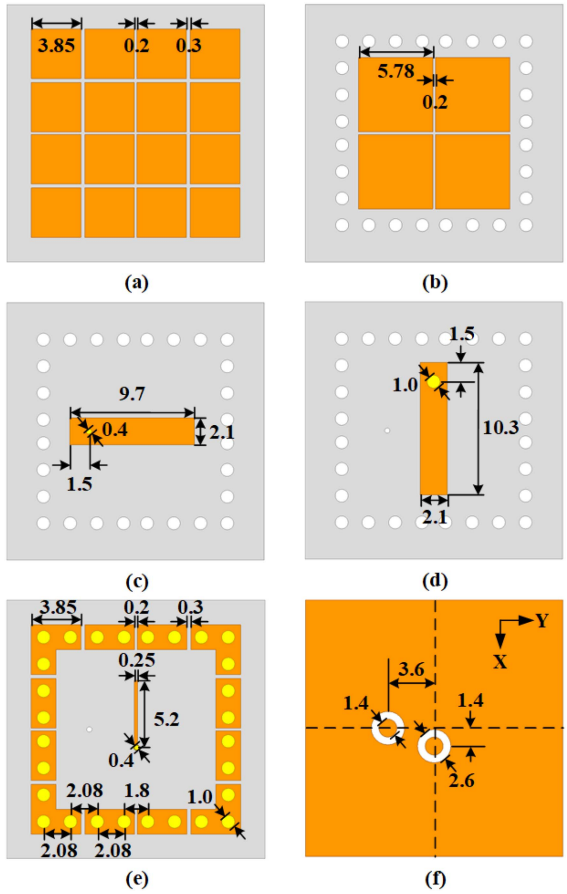

Fig. 3. Top view and geometric dimensions of the proposed DBCP antenna on (a) layer 1, (b) layer 2, (c) layer 3, (d) layer 4, (e) layer 5, and (f) ground.

miniaturization. Two L-shaped probes are orthogonally stacked to synthesize a CP wave. The results show that the antenna operates in dual bands of 6.25–6.74 GHz and 7.92–8.17 GHz with total efficiency over −6 dB (25%) and axial ratio (AR) below 2 and 4 dB, respectively. The two operating bands coincide with Channels 5 and 9, according to the UWB standards of IEEE 802.15.1-2015 and 802.15.4 z. Compared with a similar design in [19], this work adds a parasitic patch to have more freedom of dual-mode tuning, adopts a new stacked feeding network without an additional ground layer to achieve a thickness reduction of 15%, and provides an easy extension to switch to dual-linear polarization.

II. Antenna Configuration

The exploded view of the proposed DBCP antenna is shown in Fig. 2. The substrate is made of LCP with $\varepsilon_r = 2.9$ and $\tan\delta = 0.002$. This five-layer dielectric has an ultrathin profile of 0.6 mm ($0.013\lambda_0$), with each layer's thickness labeled in Fig. 2. Such strict requirements of the profile are set to adjust the extremely limited space between the back cover and the battery module in mobile handsets. Both the dielectric and the antenna structures are under a 0.8 mm thick glass cover, where we use the WL TP-1/2 material with $\varepsilon_r = 7$ and $\tan\delta = 0.002$. Top views of each layer and detailed dimensions are given in Fig. 3.

Specifically, the antenna consists of a gridded patch, a parasitic patch, a round of capacitive via fence, and a stacked feeding network. The top 4×4 gridded patch is on the upper side of layer 1, which can operate at the TM_{10} mode and the antiphase TM_{20} mode for dual-band broadside radiation. The bottom 2×2 one is placed on the upper side of layer 2. Both patches are symmetric along the x- and y- axes. A round of via fence is loaded through layers 1–4, with its top connected with the 4×4 gridded patch and its bottom surface on the upper side of layer 5. To feed the patch effectively with a complete ground, a stacked feeding network consisting of two stacked orthogonal L-shaped probes and a section of metal strip is used on the upper side of layers 3–5 separately. Each L-shaped probe excites the LP radiation along its direction. The whole antenna can be fed by a typical differential-port chip to obtain CP radiation. The software Ansoft high-frequency structure simulator (HFSS) is used for antenna design and optimization.

III. Design Process

First, in LP design, the evolution of the antenna is shown in Fig. 4. With such a low profile, common dual-band methods of using stacked configurations may face severe coupling between two layers, thus failing to separate two bands. Instead, we adopt the single-layer gridded patch for dual-band operation. As a start, Ant. 1 is a 4×4 gridded patch fed by an L-shaped probe. The initial structure has a large footprint and single wideband radiation with two resonances, the TM_{10} mode and the antiphase TM_{20} mode. The E-field distributions at the cross section are depicted in Fig. 4(c). At the lower resonance, the field exhibits a half-wavelength mode along the x-axis, which means that the TM_{10} mode is excited. As for the higher one, an antiphase E-field at the center is clearly observed, and each half-side presents a half-wavelength mode. Therefore, the antiphase TM_{20} mode is obtained. Herein, "TM" means the magnetic fields are transverse to the normal direction. Since both modes have antiphase E-fields at two sides of the aperture, the equivalent magnetic

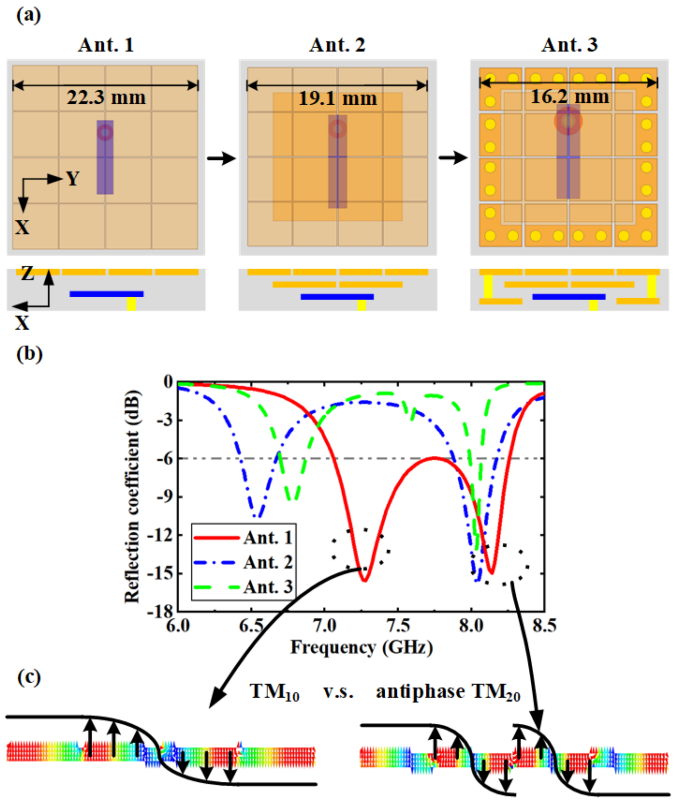

Fig. 4. Dual-band and miniaturization design. (a) Structural evolution. (b) Reflection coefficients of Ant.1 to Ant. 3. (c) E-field distributions at two resonances of Ant. 1.

currents are in phase, leading to a consistent broadside radiation pattern in both bands.

To realize dual-band operation at the specific two UWB channels using the two modes, a parasitic 2×2 patch is introduced under the top one for frequency tuning and miniaturization, which is Ant. 2. The parasitic patch introduces distributed capacitance where the E-fields at two modes have different strengths, thus changing the frequency ratio, as shown in Fig. 4(b). Compared with a similar stacked structure in [13], the two layers are so close (0.15 mm, $0.003\lambda_0$) that the parasitic large capacitance mainly works for frequency tuning, while the distance in [13] is much larger and the effect is using the relatively small capacitance for impedance matching. Different design configurations lead to different principles. For further size reduction, a round of via fence is loaded near the aperture of the patch. The fence is equivalent to a parallel capacitance at the aperture, which can concentrate and strengthen the E-field, thus reducing the size of the patch. It is noteworthy that the vias do not directly connect the patch with the ground like the substrate-integrated waveguide but leave a gap for capacitance. Actually, by changing the distance between the bottom surface and the ground plane, the equivalent capacitance can be controlled, and so does the extent of miniaturization. The tuning feasibility benefits the design under different requirements of space.

Next, based on the symmetric structure of Ant. 3, it can be extended to a CP one by simply stacking two feeding probes orthogonally. However, due to the different heights of the L-shaped probes, perturbation of the geometric parameters is needed to balance the performance in two directions. Next, a

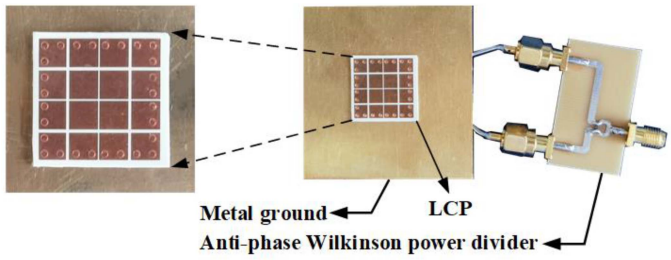

Fig. 5. Photograph of the fabricated prototype of the antenna.

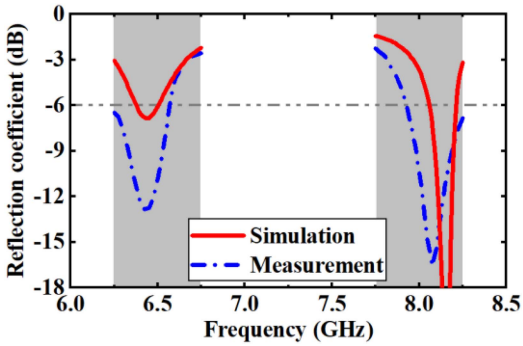

Fig. 6. Reflection coefficients of the antenna.

section of metal strip is added under the L-shaped probe in the x-direction, acting as a transmission line. Considering the effect of the feed port, the length is optimized in HFSS to provide a 90° phase difference at 7.25 GHz, the midpoint of two bands. The realistic length is shorter than the ideal quarter wavelength due to the additional capacitance of the coaxial port. To better adjust the configurations of mobile handsets, differential feed is adopted in the design and set at two ports in simulation to imitate the differential-port chip, which is widely used in digital signal processing. It is noteworthy that the design procedure implies an easy extension of the CP antenna to transform into a dual-polarized (DP) one, which also has various applications in mobile handsets.

IV. Results

To validate the design, a prototype of the antenna is fabricated and tested. As shown in Fig. 5, the antenna is located on the LCP substrate of 18 mm × 18 mm × 0.6 mm. The metal ground and the omitted glass cover have the same area of 140 mm × 70 mm. The antenna is connected to a Wilkinson power divider by two semigrid cables to imitate the differential-port chip for convenience. Two kinds of power dividers with different arm lengths are used to provide differential signals in two bands, respectively. The S-parameters are measured with a vector network analyzer (Agilent N9917A), and the radiation properties are measured in an anechoic chamber.

The reflection coefficient of the antenna is plotted in Fig. 6. The simulated result shows the −6 dB impedance bandwidth of 6.38–6.48 GHz and 8.05–8.21 GHz. The measured one is wider due to the loss of the resistor in the power divider. Besides, the isolations of a three-element array placed, as shown in Fig. 1, with an edge-to-edge distance of only 2.6 mm are also measured, which are all over 15 dB. For realistic applications in mobile devices, a differential-port chip will be used instead, excluding

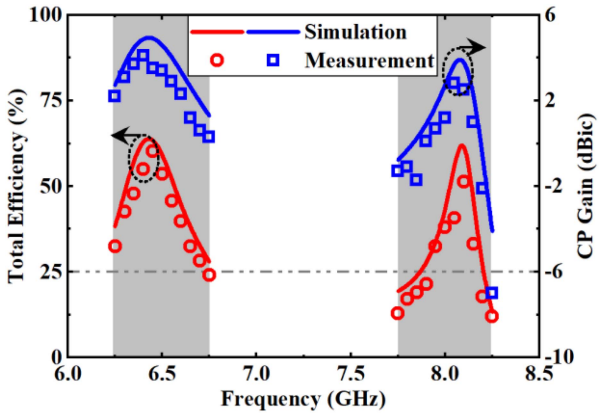

Fig. 7. Total efficiency and CP gain of the antenna.

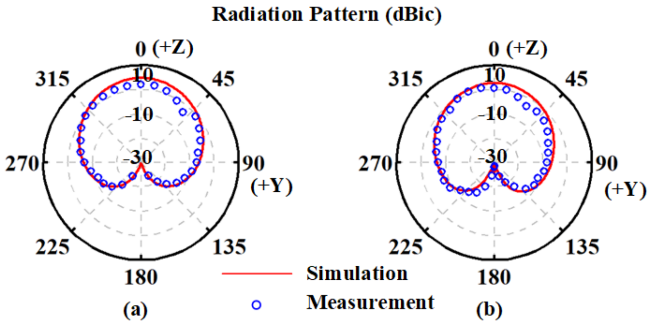

Fig. 8. Radiation patterns of the antenna at (a) 6.5 and (b) 8 GHz.

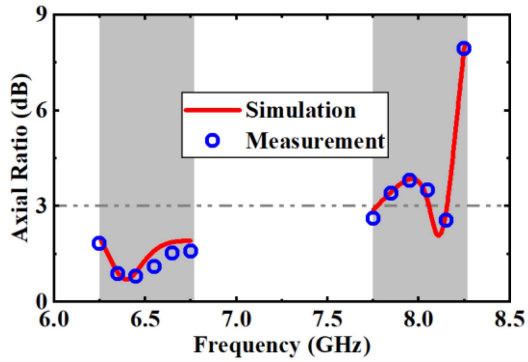

Fig. 9. AR of the antenna.

TABLE I
PERFORMANCE COMPARISON

Ref.	Profile (λ_L)	Footprint (λ_L^2)	Impedance Bandwidth	3 dB AR Bandwidth
[7]	0.086	0.46 × 0.46	16.0%; 12.5%	6.9%; 0.6%
[9]	0.065	0.36 × 0.30	16.2%; 11.3%	2.1%; 2.0%
[19]	0.015	0.34 × 0.34	7.6%*; 4.4%*	7.6%; 4.4%
[22]	0.026	0.96 × 0.83	6.3%; 8.1%	10.2%; 7.7%
Proposed	**0.013**	**0.35 × 0.35**	**7.5%*; 3.1%***	**7.5%; 1.2%**

λ_L: free-space wavelength at the center frequency of the lower band.
*: bandwidth of efficiency > −6 dB (25%).
The bold values represent the superiority of the proposed work.

the unideal factors of the power divider causing the difference between simulation and measurement. The total efficiency is given in Fig. 7 with the CP gain. It is noteworthy that, in such an extreme condition, the standard of efficiency can be usually set at −6 dB (25%). Based on this rule, the efficiency is satisfied in 6.25–6.74 GHz and 7.92–8.17 GHz, with bandwidths of 490 and 250 MHz, respectively. The CP gains in the two bands are 4.1 dBic at 6.40 GHz and 2.8 dBic at 8.05 GHz. The difference is mainly due to the fabrication errors and the loss of the power divider. The radiation patterns are shown in Fig. 8. The proposed antenna maintains broadside radiation pattern and the 3 dB beamwidths in dual bands are 80° and 76°. The broadside pattern also means that the radiated wave is propagating away from the human's head, ensuring safety for users.

As for the CP performance of the antenna, the AR is plotted in Fig. 9. In the lower band, the AR at boresight is below 2 dB. In the higher band, the CP performance gets worse because of the asymmetry of the feeding part. Nevertheless, the AR at boresight is still below 4 dB and the 3 dB AR bandwidth is 8.06–8.16 GHz. It is notable that the radiation performance inevitably becomes a compromise with such restricted profile ($0.013\lambda_0$) and footprint ($0.35\lambda_0 \times 0.35\lambda_0$).

For a clear comparison with other related DBCP antennas, some key information is listed in Table I. Antennas in [7] and [9] have a broader bandwidth at the expense of a much higher profile, which is unacceptable for FPC. In [22], the antenna has wider AR bandwidths, but the dimension is too large. The proposed antenna realizes an obvious reduction of both profile and footprint compared with the above designs. Furthermore, compared with the design in [19], the proposed antenna achieves a noteworthy reduction of 15% in the profile, which can increase the flexibility of the FCP while keeping similar bandwidth using the standard of efficiency. Also, the design fits the differential-port chip and is capable of extension to DP radiation by independently feeding the two ports. Therefore, the antenna has the virtues of ultrathin profile, compact size, DBCP radiation, and potential of integration with the FPC, showing superiority for various applications, such as UWB indoor positioning in space-limited mobile handsets.

V. CONCLUSION

A differential-fed DBCP antenna with an ultrathin LCP substrate is proposed in this letter. The antenna has extremely compact dimensions of $0.35\lambda_0 \times 0.35\lambda_0 \times 0.013\lambda_0$. Dual-band radiation is obtained by exciting two modes of the gridded patch along with a parasitic patch for frequency tuning. Two orthogonal stacked L-shaped probes with a section of metal strip form the feeding network and can be connected with the external differential-port chip in mobile terminals to achieve CP radiation or be readily transformed into DP radiation. Compared with the previous design, the proposed one achieves an obvious reduction in the profile, which makes it suitable for the extreme thickness of the FPC. The measured results show that the proposed antenna covers the dual bands of 6.25–6.74 GHz and 7.92–8.17 GHz with total efficiency over −6 dB (25%). With the merits of ultrathin profile, DBCP radiation properties, and potential integration with the FPC, the proposed antenna shows the potential for UWB indoor positioning and other various applications in space-limited mobile handsets.

REFERENCES

[1] S. Gezici and H. V. Poor, "Position estimation via ultra-wide-band signals," *Proc. IEEE*, vol. 97, no. 2, pp. 386–403, Feb. 2009.

[2] S. Gezici et al., "Localization via ultra-wideband radios: A look at positioning aspects for future sensor networks," *IEEE Signal Process. Mag.*, vol. 22, no. 4, pp. 70–84, Jul. 2005.

[3] F. Zafari, A. Gkelias, and K. K. Leung, "A survey of indoor localization systems and technologies," *IEEE Commun. Surveys Tuts.*, vol. 21, no. 3, pp. 2568–2599, Jul./Sep. 2019.

[4] X. Gao and Z. Shen, "UHF/UWB tag antenna of circular polarization," *IEEE Trans. Antennas Propag.*, vol. 64, no. 9, pp. 3794–3802, Sep. 2016.

[5] X. Shan and Z. Shen, "Miniaturized UHF/UWB tag antenna for indoor positioning systems," *IEEE Antennas Wireless Propag. Lett.*, vol. 18, no. 12, pp. 2453–2457, Dec. 2019.

[6] W. An, Z. Shen, and J. Wang, "Compact low-profile dual-band tag antenna for indoor positioning systems," *IEEE Antennas Wireless Propag. Lett.*, vol. 16, pp. 400–403, 2017.

[7] Nasimuddin, Z. N. Chen, and X. Qing, "Dual-band circularly polarized S-shaped slotted patch antenna with a small frequency-ratio," *IEEE Trans. Antennas Propag.*, vol. 58, no. 6, pp. 2112–2115, Jun. 2010.

[8] Y. Xu, L. Zhu, and N.-W. Liu, "Design approach for a dual-band circularly polarized slot antenna with flexible frequency ratio and similar in-band gain," *IEEE Antennas Wireless Propag. Lett.*, vol. 21, no. 5, pp. 1037–1041, May 2022.

[9] C. Deng, Y. Li, Z. Zhang, G. Pan, and Z. Feng, "Dual-band circularly polarized rotated patch antenna with a parasitic circular patch loading," *IEEE Antennas Wireless Propag. Lett.*, vol. 12, pp. 492–495, 2013.

[10] Q. Liu, J. Shen, H. Liu, and Y. Liu, "Dual-band circularly-polarized unidirectional patch antenna for RFID reader applications," *IEEE Trans. Antennas Propag.*, vol. 62, no. 12, pp. 6428–6434, Dec. 2014.

[11] W. Liu, Z. N. Chen, and X. Qing, "Metamaterial-based low-profile broadband aperture-coupled grid-slotted patch antenna," *IEEE Trans. Antennas Propag.*, vol. 63, no. 7, pp. 3325–3329, Jul. 2015.

[12] W. Sun, Y. Li, Z. Zhang, and P.-Y. Chen, "Low-profile and wideband microstrip antenna using quasi-periodic aperture and slot-to-CPW transition," *IEEE Trans. Antennas Propag.*, vol. 67, no. 1, pp. 632–637, Jan. 2019.

[13] W. Sun, Y. Li, L. Chang, H. Li, X. Qin, and H. Wang, "Dual-band dual-polarized microstrip antenna array using double-layer gridded patches for 5G millimeter-wave applications," *IEEE Trans. Antennas Propag.*, vol. 69, no. 10, pp. 6489–6499, Oct. 2021.

[14] K. Li, L. Li, Y.-M. Cai, C. Zhu, and C.-H. Liang, "A novel design of low-profile dual-band circularly polarized antenna with meta-surface," *IEEE Antennas Wireless Propag. Lett.*, vol. 14, pp. 1650–1653, 2015.

[15] Z. Wang and Y. Dong, "Circularly polarized antennas inspired by dual-mode SIW cavities," *IEEE Access*, vol. 7, pp. 173007–173018, 2019.

[16] K.-L. Wong and T.-W. Chiou, "Broad-band single-patch circularly polarized microstrip antenna with dual capacitively coupled feeds," *IEEE Trans. Antennas Propag.*, vol. 49, no. 1, pp. 41–44, Jan. 2001.

[17] Y. He and Y. Li, "Dual-polarized microstrip antennas with capacitive via fence for wide beamwidth and high isolation," *IEEE Trans. Antennas Propag.*, vol. 68, no. 7, pp. 5095–5103, Jul. 2020.

[18] Z. Liu, Y. Zhang, Y. He, and Y. Li, "A compact-size and high-efficiency cage antenna for 2.4-GHz WLAN access points," *IEEE Trans. Antennas Propag.*, vol. 70, no. 12, pp. 12317–12321, Dec. 2022.

[19] Y. Zhang, Y. Li, M. Hu, P. Wu, and H. Wang, "Dual-band circular-polarized microstrip antenna for ultra-wideband positioning in smartphones with flexible liquid crystal polymer process," *IEEE Trans. Antennas Propag.*, vol. 71, no. 4, pp. 3155–3163, Apr. 2023.

[20] J. Papapolymerou, "Liquid crystal polymer (LCP): A new organic material for the development of multilayer dual-frequency/dual-polarization flexible antenna arrays," *IEEE Antennas Wireless Propag. Lett.*, vol. 4, pp. 22–26, 2005.

[21] I.-J. Hwang, J.-I. Oh, H.-W. Jo, K.-S. Kim, J.-W. Yu, and D.-J. Lee, "28 GHz and 38 GHz dual-band vertically stacked dipole antennas on flexible liquid crystal polymer substrates for millimeter-wave 5G cellular handsets," *IEEE Trans. Antennas Propag.*, vol. 70, no. 5, pp. 3223–3236, May 2022.

[22] Xue Chen, L. Han, X. Chen, and W. Zhang, "Dual-band circularly polarized antenna using mu-negative transmission lines," *IEEE Antennas Wireless Propag. Lett.*, vol. 17, no. 7, pp. 1190–1194, Jul. 2018.